Figure 10 shows the debonding length as a function of the crack opening for several sets of parameters of the steel-concrete interface law (see table 3). The experimental results correspond to the dashed-line. The debonding length obtained from the modelling is close to the experimental measures. The steel-concrete debonding can be represented by cohesive elements with a debonding law. A sensitivity analysis highlights the importance of the peak stress position compared to the other two parameters α and β in the debonding law.

*Tableau 2 Parameters for the debonding law*

| CZM_LAB_MIX | a(mm) | α | β |
|---|---|---|---|
| P1 | 1 | 0.5 | 2 |
| P2 | 1 | 0.1 | 8 |
| P3 | 0.6 | 0.5 | 2 |

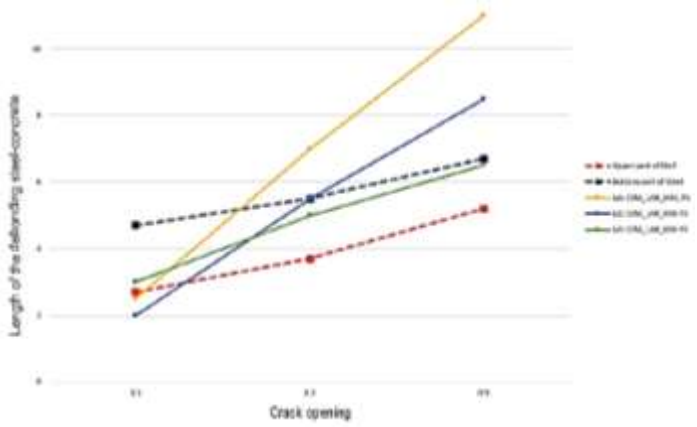


*Figure 10: Length of debonding vs crack opening*

The debonding length is correctly predicted for different crack opening values. As a consequence, it validates the debonding law and the assembly of the interface elements for concrete cracking and for the steel-concrete debonding.

## 3.2 Prediction global and local response of RC Structure

In this section, behaviour of a reinforced concrete beam is simulated and compared to experimental and numerical results in terms of force-displacement curves and number of cracks and their widths. The beam considered is the MECA beam [18]. The beam's dimensions are 5.4 m × 0.5 m × 0.2 m and the reinforcement are shown in figure 11. The beam is loading to 3 point bending.

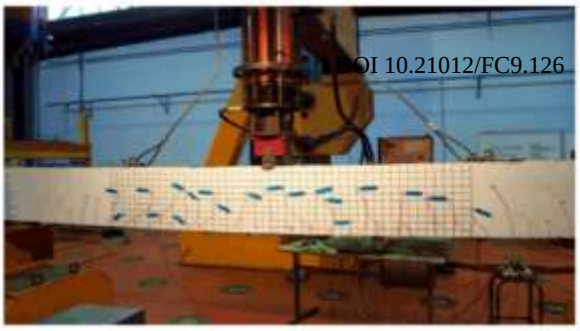


*Figure 11 : Experimental test of the beam in the three-point bending*

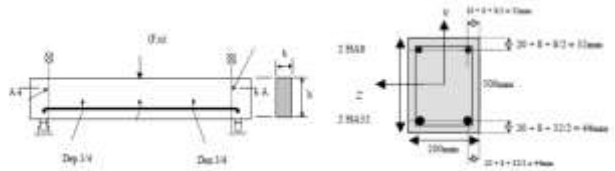

*Figure 12 Schema of the reinforcing steel in the beam*

The reinforcements are represented by two horizontal planes of membrane elements. The steel-concrete debonding is modelled using mixed interface elements with the debonding law presented in section 2.2. In order to verify the space discretization's convergence of the model, different meshes are created using 6, 9, 24 and 49 equidistant cohesive surfaces.
The boundary conditions of the beam are depicted in Figure 13. The material parameters are detailed in table 3.

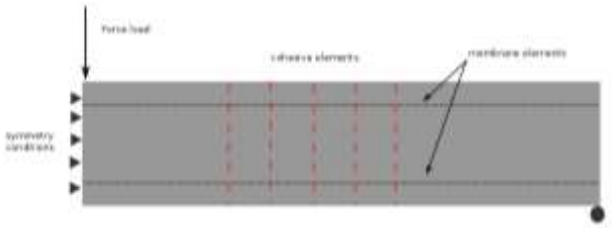


*Figure 13: Boundary conditions*

*Table 3 : Concrete parameters*

| E | ν | $\sigma_t$ | $G_f$ |
|---|---|---|---|
| 37.2GPa | 0.2 | 3.68 MPa | 100 N/m |

Figure 14 shows the deformed configuration of the beam using 24 cohesive cracks for three levels of loading. The first open cracks are concentrated in the central part of the beam, as in the experimental test, whereas at the end of the test, the open cracks are uniformly distributed on the three quarters of the beam. In figure 15, the loading versus the vertical displacement of the beam is shown for the different meshes and

compared to the experimental results. An increase in the number of cohesive surfaces decreases the beam's resistance to flexion and reduces the differences between the numerical and the experimental curves. Beyond 24 cohesive surfaces, the behaviour of the beam does not evolve and the number of open cracks remains constant. For 24 and 49 cohesive cracks, the number of open crack does not exceed 16 (Table 4) and the average opening displacement converges to 230 µm. In conclusion, if the number of cohesive planes is sufficiently large enough, the behaviour of the beam does not evolve anymore and is close to the experimental results.

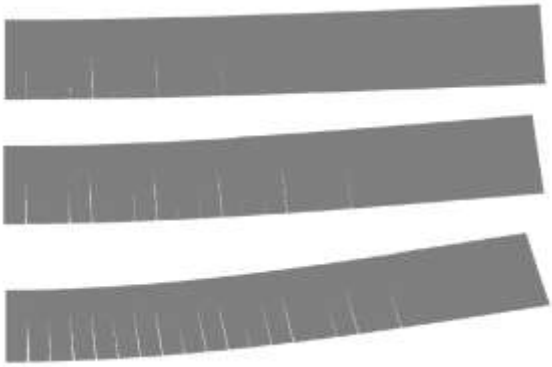

*Figure 14 : Representation of the flexion of the beam with 24 cracks for 3 levels of loading*

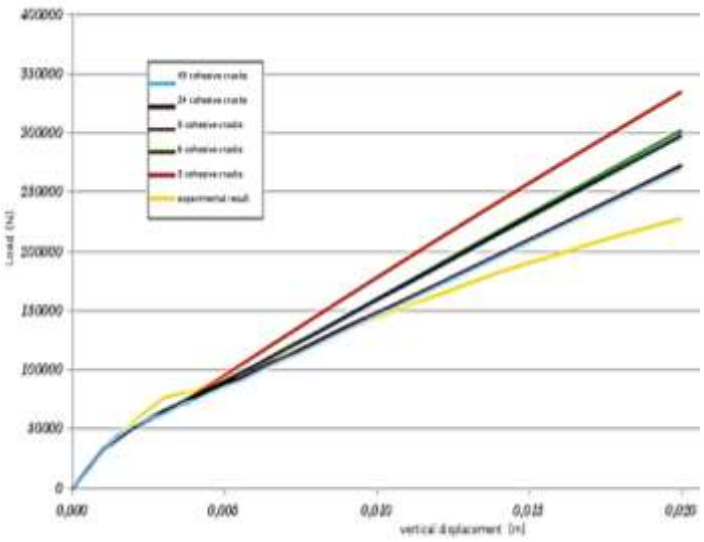


*Figure 15 : Comparison of the beam behaviour for different number of cracks*

*Table 4 Results of the numerical test*

| Number of cohesive cracks | Number of opened cracks | Opening maximum (µm) | Average opening (µm) |
|---|---|---|---|
| 49 | 16 | 420 | 230 |
| 24 | 16 | 520 | 234 |



However, a space discretization with a minimum number of elements between each cohesive surface must be respected in order to have an accuracy on stress fields. An increase in the number of potential cracks involves the number of finite elements in the mesh. A trade-off must be chosen in order to obtain a sufficiently well-represented beam behaviour while limiting simulation time.

## 3.3 Description of a prestressed concrete structure and evolution of opening cracks

### 3.3.1 Description of the test [18]

In 2005, EDF R&D and the MPA Karlsruhe decided to cooperate in project « PACE1450 » [18], which's goal is to investigate the behaviour of a curved specimen representative of a 1450 MWe nuclear power plant containment under accidental loading conditions. The specimen has realistic dimensions and therefore can be loaded very similarly to a closed ring under internal pressure. It is designed as a cut-out of the cylindrical part of a pre-stressed nuclear reactor containment (see Fig.16).

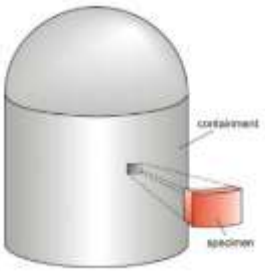


*Figure 16 The specimen is cut out of the cylindrical part of the containment [18]*

The dimension of the specimen is 2.4 m x1.8m x1.2m. It is pre-stressed using four horizontal cables consisting each of 37 strands. A vertical prestressing cable is inserted in the specimen but no load is applied. The inner and outer reinforcing grids have a diameter of 20 mm, with a spacing of 200 mm as shown in Fig 17.

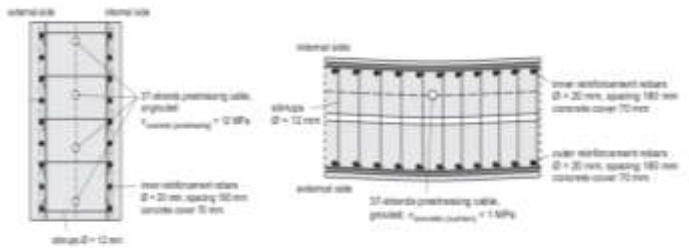

*Figure 17 : Sections of the specimen as part of the containment*

The externally applied tensile force corresponds to the ring tensile force coming from the internal pressure within the reactor containment under inspection or accidental conditions. Each test of the specimen is named “RUN”. The membrane force that would occur in a closed ring under internal pressure is enforced by hydraulic jacks pushing apart the so called “ears” which are transverse beams made of steel. They are connected to the specimen by reinforcement bars and load the specimen with the tensile force.

*Figure 18:PACE 1450*

For practical reasons, in order to speed up creep and its effects on the post-tensioning system, the pre-stressing forces have been gradually decreased in time (see Table 5). At the RUN 4, the specimen has been subjected to a pressure of 6 bar up to the creation of the cracks. After the RUN 4, many sensors have been added on the cracks in order to measure the opening of the cracks during the tests, in particular during the RUN 6, 17 months later.

*Table 5 : Test Program*

| | RUN1 | RUN2 | RUN3 | RUN4 | RUN5-6 |
|---|---|---|---|---|---|
| Prestress. | 100% | 80% | 60% | 60% | 60% |
| Pressure | 5.3 bar | 5.3 bar | 5.3 bar | 6 bar | 6 bar |
| Time | 2.5 months | 3.5 months | 5.5 months | 14 months | 21-31 months |

### 3.3.2 Modelisation of PACE 1450

The vertical prestressing tendon is modeled in 3D and the reinforcement grids and horizontal prestressing tendons are represented by membrane elements. The steel-concrete debonding is represented by a mixed interface element with the debonding law presented in section 2.2. The cracks pass straight through the structure, from the inside to the outside. Five potential cracks are integrated as 5 plans of cohesive elements into the mesh. The behavior associated with these elements is the exponential cohesive law. The creep model for the concrete is detailed in [18].

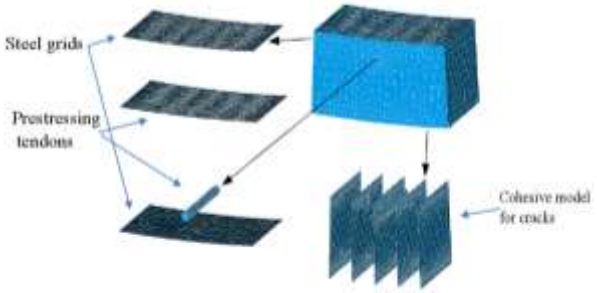


*Figure 19 : Mesh of PACE 1450*

*Table 6 : Parameters of the different laws*

| Concrete parameters | | Exponential Law | |
|---|---|---|---|
| E | 26 GPa | $\sigma_t$ | 3 MPa |
| ν | 0.22 | $G_f$ | 100 N/m |
| Steel parameters | | Debonding Law | |
| E | 200GPa | (α,β) | (0.5,1) |
| ν | 0.3 | $\tau_m$ | 10 MPa |
| | | $a_m$ | 1 mm |

The prestressing values are given in Table 5. Figure 20 represents the loading applied during RUN 6. The loading applied during RUN 4 and the RUN 6 are similar. The successive steps of pressure are: 4 bar, 5 bar, 5.5 and 6 bar. The opening of one crack, C15, is also shown in Figure 20.

DOI 10.21012/FC9.126

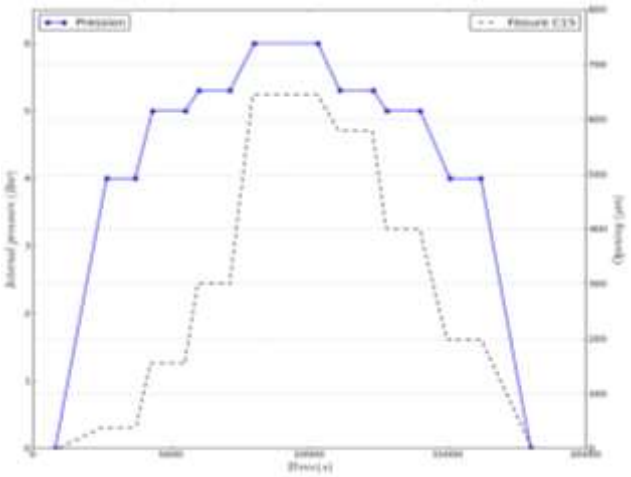

*Figure 20 : Pressure scenario during RUN 6 with measured crack opening C15*

The simulation of the PACE1450 test is realized from the concreting of the specimen up to the date of RUN6, 31 months later. All variations of prestressing and all mechanical tests (RUN1-6) are taken into account.

The initiation of cracks during the RUN4 test is simulated. Two cracks are predicted on the 4th and 5th cohesive plan and the cracks opening are as expected. The opening of these two cracks during the test RUN6 is compared to experimental data from two cracks in Figure 21. The cracks C15 and C11 are observed in the experimental test. Their openings are similar to the opening of the 4th and 5th cohesive element plan. The opening between the experimental and numerical results are consistent but not identical.

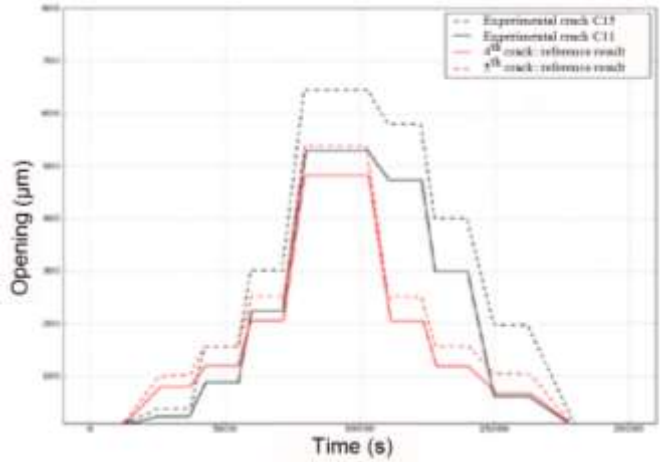


*Figure 21 : Measured and simulate crack openings during RUN 6*

The combination of the mixed interface finite element for the crack and the steel-concrete debonding and the creep model can simulate the behavior of a prestressed concrete structure, the crack openings during the RUN4 and the reopening during the RUN6. However the abrupt opening of the plans of cohesive element and the sensitivity of the results with respect to the boundary conditions make it difficult the simulation of the crack during the RUN4.

## 4 Simulation of a part of the containment building with an initial pre-crack state

So far, it was shown that tools for simulating the cracking of concrete structures are available. Nevertheless, in some cases, it could be difficult to obtain the crack pattern observed on a structure by a simulation, especially for industrial structures. This difficulty could come from the misunderstanding of the loads applied on the structure, the influence of the material heterogeneities or the convergence difficulties. In this case, it seems interesting to be able to define an initial pre-cracked state for a concrete structure and to study only the evolution of the crack and not the occurrence of this cracks.

Thus, a definition of an initial cracked state is proposed and validated with the experimental test PACE1450. The advantages of the test PACE1450 are :

- Dimension and reinforcement of the steel corresponding to a confinement vessel
- Several cracks are created under a known load
- These cracks are reopened under the same load few months later and the surface openings were measured

The results from section 3.3 is considered as the reference calculation. A comparison between the reference calculation and a result which starts after the cracking of the specimen with the initial pre-crack state is proposed.

### 4.1 Definition of the initial pre-crack state

It is assumed here that at the date of the RUN4, cracks are present and their locations are know from observations. Then we want to predict the openings cracks 17 months later (equivalent to the RUN6).

The analysis is performed in two steps:

- A preliminary simulation is performed from concreting up to RUN4 (14 months), considering only creep and not cracking or decohesion in the structure. The mesh is thus very simple: 3D elements for the

concrete and membrane elements for the steels. At the end of the RUN 4, the stress field, the displacement field and the state variables for the creep model are determined.

- For the second simulation, Two cohesive cracks are introduced in the mesh (corresponding to the 4th and 5th cracks of the model) and the decohesion between concrete and steel.

The initial state is defined as :

- For the concrete and the steels by projecting the stress field and the state variables of the preliminary simulation
- For the two cracks, by assuming that they are closed but fully damaged
- For the steel-concrete bond, by assuming the evolution of the slip near the vertical cracks. This evolution has been determined thanks to the observation of the results obtained in section 3.3 and figure 22 in order to obtain the following relation :

$$\xi(x) = \xi_{max} \frac{l-x}{l-p} \qquad (13)$$

With $\xi_{max}$ being the maximum debonding of the interface, l the debonding length and p the position of the crack.

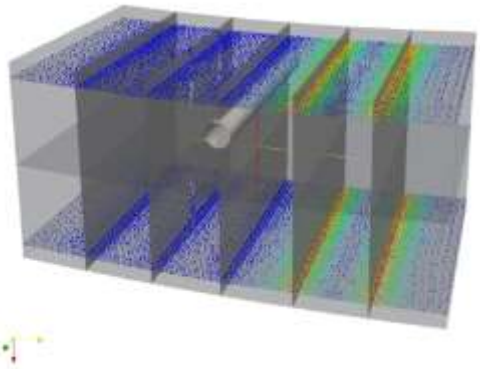

*Figure 22: Visualization of the slip between steel and concrete*

### 4.2 Analysis of the results

Figure 23 compares the opening of the 4th and the 5th cohesive element plan for the two types of analysis: the reference simulation and the calculation with an initial pre-crack state. The profiles of the two curves are very similar and the difference of the opening is at most 40 µm. This difference may come from the damage around the horizontal tendon that is not introduced in the initial pre-crack state.

DOI 10.21012/FC9.126

The initial pre-crack state allows us to reproduce the opening of cracks during the RUN 6 with the following informations: position of the cracks, behaviour of concrete and an estimation of the steel-concrete debonding.

Using a simplified mesh without simulating the openings cracks until RUN 4 reduces the computing time by 30%. The time duration until RUN 4 and between RUN 4 and RUN 6 are equally long (Table 5). In the case of a later appearing cracking structure, the speed-up is greater.

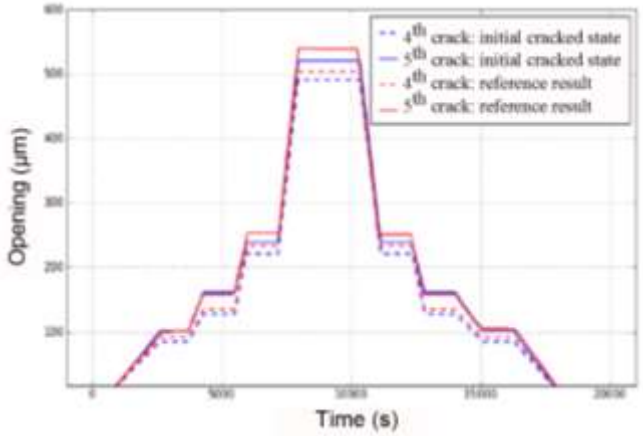


*Figure 23 Evolution of the cracks openings during run 6 : Comparison between the reference calculation and method of crack insertion*

## 5 Conclusion

In this article, we shown that cohesive zone models could be used to describe both the steel-concrete debonding and the cracking phenomena in reinforced concrete structures. Indeed, three structures have been simulated and compared to experimental results. Satisfactory results have been obtained both at the global and local scales, if the number of potential cracks and the discretization are sufficient.

As it is sometimes difficult to get a realistic crack pattern for industrial structures, we have proposed a methodology to define initial the pre-crack state of the structure. It should allow to study the evolution of the crack without simulating its occurrence. The applicability has been demonstrated on the PACE1450 experiment. Other examples are in progress, and in particular the study of other local zones of the containment vessels, that could be cracked specially during the early age due to shrinkage phenomena.

## REFERENCES


[1] Owen, D. and Hinton, 1980. Finite elements in plasticity: Theory and practice. *Pineridge Press* Lt

[2] Laborderie, C. 1991. Phénomènes unilatéraux dans un matériau endommageable: modélisation et application à l'analyse des structures en béton. *PhD Thesis*

[3] Lorentz, E. 2004.Localization phenomena and regularization methods. *Local Approach to Fracture*. Paris, Les Presses de l'Ecole des Mines

[4] Jendele, L. and Červenka, J. 2009. On the solution of multi-point constraints – Application to FE analysis of reinforced concrete structures. *Computers & Structures, Volume 87*, Issues 15–16, August.

[5] David M., 2012, Approche multi-échelle du comportement mécanique des structures en béton armé - Application aux enceintes de confinement des centrales nucléaires, Phd Thesis. *Laboratoire Mécanique des Solides de Polytechnique*

[6] Sanahuja, J., Dormieux, L. and Chanvillard G. 2007. Modelling elasticity of a hydrating cement paste. *Cement and Concrete Research*, 37(10), 1427–1439,

[7] Mazars, J. 1986. A description of micro and macroscale damage of concrete structure. *Engineering Fracture Mechanics*, Vol25, p729-737.

[8] Lorentz, E. and Andrieux S. 1999. A variational formulation for nonlocal damage models. *International Journal of Plasticity* 15(2), 119-138

[9] Lorentz, E. 2008. A mixed interface finite element for cohesive zone models. *Computer Methods in Applied Mechanics and Engineering 198.2*

[10] Francfort G.A., Marigo J.-J., Revisiting brittle fracture as an energy minimization problem, *Journal of the Mechanics and Physics of Solids*, Volume 46

[11] Petersson, P.E. 1980, Fracture energy of concrete: Practical performance and experimental results, *Cement and Concrete Research*, Volume 10

[12] Cazes F. 2010. Construction et implementation de lois cohésives extrinsèques, *PhD Thesis*

[13] Needelman, A. 1987. A continuum model for void nucleation by inclusion debonding. *Journal of Applied Mechanic*s. 54(3)

[14] Alfano, G. 2006 On the influence of the shape of the interface law on the application of cohesive zone models. *Journal Composite Sciences and Technology*. Volume 66, Issue 6

DOI 10.21012/FC9.126

[15] Goto Y. 1971. Cracks Formed in Concrete Around Deformed Tension Bars, *Journal Proceedings*. Volume 68-4

[16] Eligehausen, R., Popov, E. and Bertero, V. 1983. Local bond stress-slip relationships of deformed bars under generalized excitations, *Technical Report UCB/EERC-83/23 of the National Science Foundation*, University of California, Berkeley

[17] Ghantous, R.M., Millard A., Poyet S., François R., L'Hostis V. and Tran N.C, 2016, Experimental and numerical characterisation of load-induced damage in reinforced concrete members. *Proceedings of the international conference: 9th FramCos*, Berkeley, USA

[18] Ghavamian, S. 2003. Modèles de fissuration de béton, projet MECA. *Revue française de génie civil volume 7* – n°5/

[19] Herrmann, N., Müller, H. S., Niklasch C., Michel-Ponnelle S., Le Pape Y., Bento C., 2012, PACE-1450 The crack and leakage behavior of a prestressed concrete wall considering the prestressing loss due to aging

[20] Lorentz, E., 2005, Ill-posed boundary conditions encountered in 3D and plate finite element simulations, *Finite Elements in Analysis and Design* 41